Physica D 289 (2014) 18–31

Contents lists available at ScienceDirect

Physica D

journal homepage: www.elsevier.com/locate/physd

The Kuramoto model of coupled oscillators with a bi-harmonic coupling function

M. Komarov *, A. Pikovsky

Department of Physics and Astronomy, Potsdam University, Karl-Liebknecht-Str 24/25, 14476 Potsdam, Germany
Department of Control Theory, Nizhny Novgorod State University, Gagarin Avenue 23, 603950 Nizhny Novgorod, Russia

HIGHLIGHTS

- The Kuramoto model with a bi-harmonic coupling function was investigated.
- We develop a method for an analytic solution of self-consistent equations.
- We observed a multi-branch locking with a multiplicity of coherent states.
- Multi-branch synchronous states coexist with neutrally stable asynchronous regime.
- We show that the asynchronous state has a finite life time for finite ensembles.

ARTICLE INFO

Article history:
Received 29 April 2014
Received in revised form
30 August 2014
Accepted 3 September 2014
Available online 16 September 2014
Communicated by S. Coombes

Keywords:
Kuramoto model
Bi-harmonic coupling function
Multi-branch entrainment
Synchronization

ABSTRACT

We study synchronization in a Kuramoto model of globally coupled phase oscillators with a bi-harmonic coupling function, in the thermodynamic limit of large populations. We develop a method for an analytic solution of self-consistent equations describing uniformly rotating complex order parameters, both for single-branch (one possible state of locked oscillators) and multi-branch (two possible values of locked phases) entrainment. We show that synchronous states coexist with the neutrally linearly stable asynchronous regime. The latter has a finite life time for finite ensembles, this time grows with the ensemble size as a power law.

© 2014 Elsevier B.V. All rights reserved.

1. Introduction

Large systems of coupled nonidentical oscillators are of general interest in various branches of science. They describe Josephson junction circuits [1–3], electrochemical [4] and spin-torque [5,6] oscillators, as well as variety of interdisciplinary applications including pedestrian induced oscillations of footbridges [7], applauding persons [8], and others. Similar models are also used in biology, for example in studying of neural ensembles dynamics [9,10] and systems describing circadian clocks in mammals [11,12]. In many cases the analysis of large ensembles consisting of heterogeneous oscillators can be successfully performed in the phase approximation [13,14]. Indeed, if the interaction between the elements is weak, the amplitudes are enslaved, and the dynamics of self-sustained oscillators can be effectively described by a relatively simple system of coupled phase equations. The special case of a globally coupled network of phase oscillators (so-called Kuramoto model [13,15]) attracted a lot of attention [16] and has been established as a paradigmatic model describing transitions from incoherent to synchronous states in the ensembles of coupled oscillators.

Quite a complete analysis of the Kuramoto model can be performed in the case of a harmonic sin-coupling function [13,17,18], although even here non-trivial scenarios of transition to synchrony have been reported [19]. Less studied is the case of more general coupling functions, containing many harmonics. Here we perform a systematic study of the synchronous regimes for a bi-harmonic coupling function (see [20] for a short presentation of these results which have been later confirmed in [21]). We introduce the model and discuss previous findings in Section 2. Then in Section 3 we give a general solution of the self-consistent equations describing rotating-wave synchronous solutions. In Section 4 we give a detailed analysis of the simplest symmetric

* Corresponding author at: Department of Physics and Astronomy, Potsdam University, Karl-Liebknecht-Str 24/25, 14476 Potsdam, Germany. Tel.: +49 3319775987.
E-mail address: maxim.a.komarov@gmail.com (M. Komarov).

http://dx.doi.org/10.1016/j.physd.2014.09.002
0167-2789/© 2014 Elsevier B.V. All rights reserved.

case (no phase shifts in the coupling), while a general situation is illustrated in Section 5. In conclusion, we summarize the results and outline open questions. In this paper we focus on the deterministic oscillator dynamics, the case of noisy oscillators will be considered elsewhere [22].

2. Kuramoto model and bi-harmonic coupling

The general Kuramoto model is formulated as a system of differential equations for the phases φ_k of N oscillators:

$$\dot{\varphi}_k = \omega_k + \frac{1}{N}\sum_{n=1}^{N} \Gamma(\varphi_n - \varphi_k), \quad k = 1, \ldots, N. \tag{1}$$

All the oscillators are identical, except for diversity of the natural frequencies ω_k, distributed according to a certain distribution function $g(\omega)$. The level of coherence in the network of phase oscillators can be described by order parameters R_n, defined as:

$$R_n e^{i\Theta_n} = \frac{1}{N}\sum_{k=1}^{N} e^{in\varphi_k}, \quad n \in \mathbb{N}. \tag{2}$$

The state with $R_n = 0$ for all n corresponds to a purely incoherent dynamics (uniform distribution of the phases), while non-zero values of at least some order parameters indicate for certain synchrony in the ensemble. In the case of pure sinusoidal coupling, $\Gamma(x) = \varepsilon \sin(x + \alpha)$, the original analysis by Kuramoto [15,13] and its subsequent extensions [23–25,17,18] revealed a clear picture of a transition from an asynchronous state to coherence in the thermodynamical limit $N \to \infty$. It was shown that above certain critical value of the coupling ($\varepsilon > \varepsilon_c$), the system undergoes a transition from disordered behavior to synchronous collective motion via a supercritical bifurcation with the main order parameter obeying $R_1 \sim (\varepsilon - \varepsilon_c)^{\frac{1}{2}}$.

The situation is much less trivial for more general coupling functions Γ. The presence of higher harmonics in coupling function [26,24,25,27] may change scaling of the order parameter to linear law $R_1 \sim \varepsilon - \varepsilon_c$. Moreover, as has been already mentioned in an early paper by Winfree [28] and in subsequent numerical studies by Daido in [29,30], sufficiently strong higher modes in the coupling function Γ may cause a so-called multibranch entrainment, in which a huge number of stable or multistable phase-locked states exist. In certain cases the interplay between synchronizing action of one coupling mode and repelling force from another one can be a reason for an oscillatory behavior of macroscopic order parameters [31].

This paper is devoted to a systematic study of the Kuramoto model in the case of a general bi-harmonic coupling function

$$\Gamma(x) = \varepsilon \sin(x - \beta_1) + \gamma \sin(2x - \beta_2) \tag{3}$$

in the thermodynamic limit $N \to \infty$. In Section 3 we formulate an analytic self-consistent approach [15,13,32] which allows us to calculate stationary or uniformly rotating order parameters $R_{1,2}$ (including all possible multi-branch entrainment states) depending on the parameters of the bi-harmonic coupling function Γ. Based on the self-consistent method, we present in Section 4 a complete diagram of uniformly rotating states with constant order parameters, for a special case of symmetric coupling function Γ ($\beta_{1,2} = 0$). Surprisingly, (i) synchronous solutions appear *prior* to the stability threshold of incoherent state; (ii) these regimes have order parameters that can take values anywhere in the range $(0, R_{max}]$ for some $R_{max} < 1$; (iii) there is a huge multiplicity of these states for fixed coupling parameters (multi-branch entrainment) which can also appear for *relatively weak* second mode (when parameter γ is small compared to absolute value of ε) in the coupling. Here we also illustrate the multiplicity of solutions, and, combining the self-consistent approach and a perturbative analysis, we derive the scaling laws of $R_{1,2}(\varepsilon, \gamma)$ near the transition points where coherent state appears.

For a general case of non-zero phase shifts $\beta_{1,2}$, consideration of the self-consistent equations becomes rather tedious due to a large number of parameters involved. We restrict our attention in Section 5 to several examples with multibranch entrainment and already mentioned oscillatory states [31].

Before proceeding with the analysis, we mention three examples of realistic physical systems where the second harmonics term in the coupling function is strong or even dominating. The first example is the classical Huygens' setup with pendulum clocks suspended on a common beam (common platform). The horizontal displacement of the beam leads to the first harmonics coupling $\sim \varepsilon$, while the vertical mode produces the second harmonics term $\sim \gamma$ [33]. We give a derivation of the phase equations for the case where both horizontal and vertical displacements of the platform are present, in Appendix, where Eq. (32) is in fact the Kuramoto model with bi-harmonic coupling. Another example are recently experimentally realized φ-Josephson junctions [34], where the dynamics of a single junction in the array is governed by a double-well energy potential. Therefore one can expect strong effects caused by the second harmonics in the interaction. The third example are experiments with globally coupled electrochemical oscillators [35,36], where a pronounced second harmonics has been observed in the coupling function inferred from the experimental data.

3. Self-consistent equations and their solution

We start our analysis with reformulation of Eq. (1) for the bi-harmonic coupling as

$$\dot{\varphi}_k = \omega_k + \varepsilon \mathrm{Im}\left[e^{-i\beta_1 - i\varphi_k}\frac{1}{N}\sum_n e^{i\varphi_n}\right] + \gamma \mathrm{Im}\left[e^{-i\beta_2 - i2\varphi_k}\frac{1}{N}\sum_n e^{i2\varphi_n}\right].$$

In the thermodynamical limit, using the two relevant order parameters $R_{1,2}e^{i\Theta_{1,2}}$, defined according to (2), we obtain:

$$\dot{\varphi} = \omega + \varepsilon R_1 \sin(\Theta_1 - \varphi - \beta_1) + \gamma R_2 \sin(\Theta_2 - 2\varphi - \beta_2). \tag{4}$$

We assume the natural frequencies ω to be distributed according to a symmetric unimodal density $g(\omega)$. Furthermore, due to rotational invariance of the problem, the mean frequency can be set to zero by virtue of a transformation into a rotating reference frame. In the thermodynamic limit the complex order parameters $R_m e^{i\Theta_m}$ can be represented using the conditional distribution function $\rho(\varphi|\omega)$:

$$R_m e^{i\Theta_m} = \iint d\varphi d\omega\, g(\omega)\rho(\varphi|\omega)e^{im\varphi}, \quad m = 1, 2. \tag{5}$$

Below we consider only the states of uniformly rotating order parameters. Let us perform the following transformation of variables to the rotating (with some frequency Ω) reference frame:

$$\Theta_1 = \Omega t + \theta_1; \qquad \Theta_2 = 2\Omega t + \theta_2; \\ \varphi = \Omega t + \theta_1 - \beta_1 + \psi, \tag{6}$$

where θ_1 and θ_2 are constants. Then Eq. (4) changes as follows:

$$\dot{\psi} = \omega - \Omega + \varepsilon R_1 \sin(-\psi) + \gamma R_2 \sin(\theta_2 - 2\theta_1 + 2\beta_1 - \beta_2 - 2\psi). \tag{7}$$

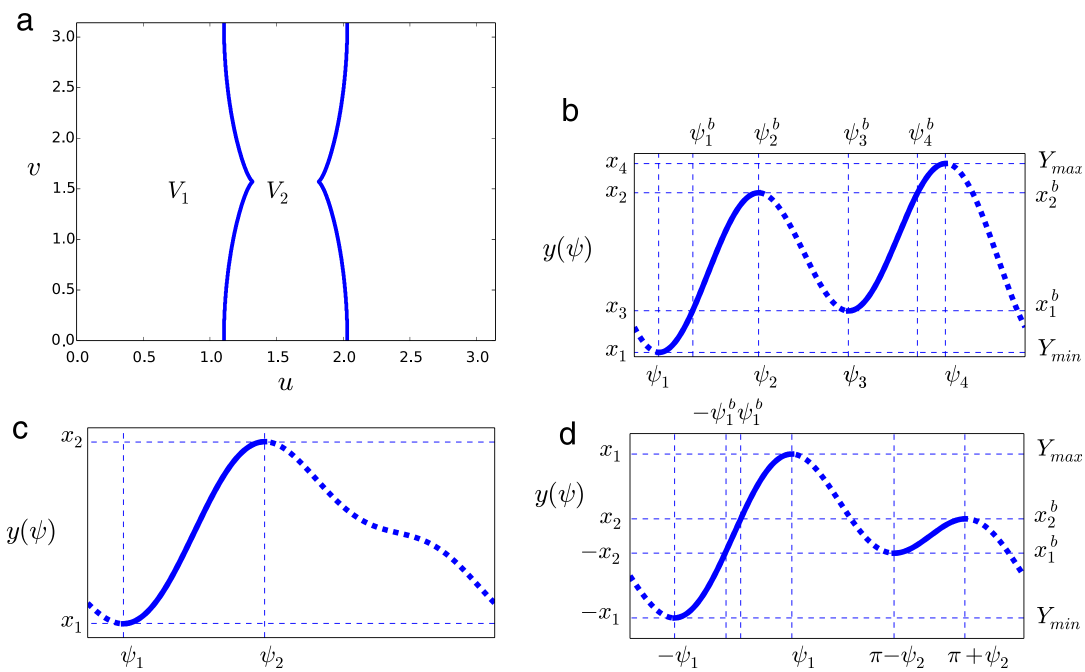

Fig. 1. (a) Regions V_1 and V_2 in the plane of parameters (u, v): Domain V_1 corresponds to a double-well form of function $y(u, v, \psi)$ (Fig. 1(b,d)), while in domain V_2 function $y(u, v, \psi)$ has a single-well form like shown in Fig. 1(c). (b) Example of function $y(u, v, \psi)$ with 4 extrema is presented. There are two stable branches (solid curves) for stationary phases of locked oscillators. The left branch $\psi = \Psi_1(x, \mathbf{P})$ is larger than the right one $\psi = \Psi_2(x, \mathbf{P})$. $(\psi_{1,2}, x_{1,2})$ denote coordinates of the extrema corresponding to the branch Ψ_1, while $(\psi_{3,4}, x_{3,4})$ denote extrema at Ψ_2. In the domain $y(\psi) \in [x_1^b, x_2^b]$ there is a bistability on the microscopic level: in this domain the oscillators can be locked either on the branch Ψ_1 in the range $\psi \in [\psi_1^b, \psi_2^b]$ or on the branch Ψ_2 in the range $\psi \in [\psi_3^b, \psi_4^b]$. (c) Example of function $y(u, v, \psi)$ with only two extrema and one stable branch $\psi = \Psi_1(x, \mathbf{P})$ (solid curve). (d) Example of function $y(u, v, \psi)$ in the special case $v = 0$. In this special case branches Ψ_1 and Ψ_2 are symmetric (see Eq. (18)). Due to the symmetry the first branch is always centered in the interval $[-\psi_1, \psi_2]$, and the second branch is centered in the interval $[\pi - \psi_2, \pi + \psi_2]$. The area of bistablity for the first branch Ψ_1 is in the interval $[-\psi_1^b, \psi_1^b]$. For the second branch the entire range $[\pi - \psi_2, \pi + \psi_2]$ (where this branch is defined) is in the area of bistability.

It is convenient to introduce a set of parameters $\{R, u, v, z\} = \mathbf{P}$ in the following way:

$$\begin{aligned} &\varepsilon R_1 = R \sin u, \qquad \gamma R_2 = R\cos u, \\ &\Omega = zR, \qquad v = \theta_2 - 2\theta_1 + 2\beta_1 - \beta_2. \end{aligned} \tag{8}$$

Now Eq. (7) takes the form:

$$\begin{aligned} \dot{\psi} &= R\,(x - z - \sin u \sin\psi - \cos u \sin(2\psi - v)) \\ &= R\,(x - z - y(u, v, \psi)). \end{aligned} \tag{9}$$

We denoted $x = \omega/R$ and $y(u, v, \psi) = \sin u \sin\psi + \cos u \sin(2\psi - v)$.

Here we summarize the meaning of all new variables and parameters:

- $\theta_1 = \Theta_1 - \Omega t$ and $\theta_2 = \Theta_2 - 2\Omega t$ are the phase shifts of the first and the second order parameters in the rotating frame.
- $\psi = \varphi - \Omega t + \beta_1 - \theta_1$ is the oscillator's phase in the rotating frame, shifted by a constant $\beta_1 - \theta_1$.
- $R = \sqrt{\varepsilon^2 R_1^2 + \gamma^2 R_2^2}$ is an overall amplitude of the coupling function. For $\varepsilon, \gamma \neq 0$, R can be zero only if both order parameters vanish $R_1 = R_2 = 0$.
- u is a parameter reflecting relative strengths of coupling terms in the first and the second harmonics: ($\sin u = \frac{\varepsilon R_1}{R}$ and $\cos u = \frac{\gamma R_2}{R}$, respectively) For example, when $u = 0$ oscillators interact only via the second harmonics ($\sim \gamma R_2$).
- $z = \Omega/R$ is the rescaled rotating frequency of the order parameters.
- $x = \omega/R$ are the rescaled individual frequencies of oscillators.
- $v = \theta_2 - 2\theta_1 + 2\beta_1 - \beta_2$ is an effective phase shift of the second harmonics coupling term with respect to the coupling at the first harmonics.
- $y(u, v, \psi) = \sin u \sin\psi - \cos u \sin(2\psi - v)$ is the rescaled coupling function.

Setting parameters $\mathbf{P}$ to some constant values in (9) (this means that $R_{1,2}, \theta_{1,2}$ are constants, i.e. the order parameters are uniformly rotating with velocity Ω), one can find a stationary distribution function $\rho(\psi|x, \mathbf{P})$ and then calculate the corresponding complex order parameters as:

$$\begin{aligned} R_1 e^{i\theta_1} &= e^{i(\theta_1-\beta_1)} R \iint dx d\psi\, \rho(\psi|x, \mathbf{P}) e^{i\psi} g(Rx) \\ &= e^{i(\theta_1-\beta_1)} R F_1(\mathbf{P}) e^{iQ_1(\mathbf{P})}, \\ R_2 e^{i\theta_2} &= e^{i2(\theta_1-\beta_1)} R \iint dx d\psi\, \rho(\psi|x, \mathbf{P}) e^{i2\psi} g(Rx) \\ &= e^{i2(\theta_1-\beta_1)} R F_2(\mathbf{P}) e^{iQ_2(\mathbf{P})}, \\ F_m(\mathbf{P}) e^{iQ_m(\mathbf{P})} &\equiv \iint dx d\psi\, \rho(\psi|x, \mathbf{P}) e^{im\psi} g(Rx), \quad m = 1, 2. \end{aligned} \tag{10}$$

Our next goal is to calculate the integrals $F_m(\mathbf{P})$, for this we need to find, using the dynamical equation (9), the distribution function $\rho(\psi|x, \mathbf{P})$. Let Y_{min} and Y_{max} denote the global minimum and the global maximum of function $y(u, v, \psi)$, respectively. (Fig. 1(b)). All the oscillators can be separated into locked ones (for $Y_{max} \geq |x - z| \geq Y_{min}$) or rotating, unlocked ones ($x - z > Y_{max}$ or $x - z < Y_{min}$). The distribution function of rotating oscillators (index r) is inversely proportional to their phase velocity:

$$\rho_r(\psi|x, \mathbf{P}) = g(Rx)\rho(\psi|x, \mathbf{P}) = \frac{C(x)}{|x - z - y(\psi, u, v)|}, \tag{11}$$

where $C(x)$ is the normalization constant to which we included also the distribution of frequencies:

$$C(x) = \frac{g(Rx)}{\int_0^{2\pi} \frac{d\psi}{|x-z-y|}}.$$

The stationary phases of locked oscillators (index l) can be found from the following relation:

$$x - z = y(u, v, \psi). \tag{12}$$

When finding ψ as a function of x, we have to satisfy an additional stability condition $\frac{\partial y(u,v,\psi)}{\partial \psi} > 0$ that follows from the dynamical equation (9). In the (u, v) plane there are two regions V_1 and V_2 (Fig. 1(a)) with qualitatively different properties of system (9) and different types of distribution function $\rho_l(\psi|x, \mathbf{P})$, correspondingly:

(i) $\{u, v\} \in V_1$. In this case function $y(u, v, \psi)$ has a double-well form like shown in Fig. 1(b). According to (12), oscillators can be located on two possible stable branches highlighted by solid curves in Fig. 1(b): the first branch is $\psi = \Psi_1(x, \mathbf{P})$ in the range $\psi \in [\psi_1, \psi_2]$ and another branch is $\psi = \Psi_2(x, \mathbf{P})$ for $\psi \in [\psi_3, \psi_4]$. Here and below we assume $\Psi_1(x, \mathbf{P})$ to be the biggest stable branch. In the range $(x - z) \in (x_1^b, x_2^b)$ (Fig. 1(b)) there is an area of bistability on the microscopic level: the oscillators with the same natural frequency x can be locked at two different phases $\Psi_1(x, \mathbf{P})$ and $\Psi_2(x, \mathbf{P})$. Therefore, the distribution function has the following form:

$$\rho_l(\psi|x, \mathbf{P}) = \begin{cases} (1 - S(x))\delta(\psi - \Psi_1(x, \mathbf{P})) + S(x)\delta(\psi - \Psi_2(x, \mathbf{P})) \\ \quad \text{for } (x - z) \in [x_1^b, x_2^b], \\ \delta(\psi - \Psi_1(x, \mathbf{P})) \quad \text{for } (x - z) \in [x_1, x_2] \setminus [x_1^b, x_2^b], \\ \delta(\psi - \Psi_2(x, \mathbf{P})) \quad \text{for } (x - z) \in [x_3, x_4] \setminus [x_1^b, x_2^b]. \end{cases} \tag{13}$$

Here $0 \le S(x) \le 1$ is an indicator function describing the redistribution over the stable branches; this function is arbitrary.

(ii) $\{u, v\} \in V_2$. In the second case, function $y(u, v, \psi)$ has only two extrema (Fig. 1(c)) and there is only one stable branch $\psi = \Psi_1(x, \mathbf{P})$. The distribution function is:

$$\rho_l(\psi|x, \mathbf{P}) = \delta(\psi - \Psi_1(x, \mathbf{P})) \quad \text{for } x \in (z + x_1, z + x_2). \tag{14}$$

Taking into account the obtained expressions for the distribution function ((11), (13) and (14)), the integrals in (10) can be rewritten as a sum of five terms:

$$\begin{aligned} F_m(\mathbf{P})e^{iQ_m(\mathbf{P})} &= \int_{\psi_1}^{\psi_2} d\psi e^{im\psi} g\left(R(z+y)\right) \frac{\partial y}{\partial \psi} \\ &- \int_{\psi_1^b}^{\psi_2^b} d\psi e^{im\psi} S(z+y) g\left(R(z+y)\right) \frac{\partial y}{\partial \psi} \\ &+ \int_{\psi_3}^{\psi_4} d\psi e^{im\psi} g\left(R(z+y)\right) \frac{\partial y}{\partial \psi} \\ &- \int_{\psi_3^b}^{\psi_4^b} d\psi e^{im\psi} \left(1 - S(z+y)\right) g\left(R(z+y)\right) \frac{\partial y}{\partial \psi} \\ &+ \int_{\mathcal{X}} \int_0^{2\pi} dx d\psi \frac{C(x)e^{im\psi}}{|x - z - y|}. \end{aligned} \tag{15}$$

Here the first and the second terms stand for integration over the first branch Ψ_1 in the range $[\psi_1, \psi_2]$. The second term accounts for certain redistribution $S(x)$ of oscillators between the branches in the range $[\psi_1^b, \psi_2^b]$ (Fig. 1(b)). Similarly, the third and the fourth terms correspond to integration over the possible stable branch Ψ_2 in the range $[\psi_3, \psi_4]$. In the same way, the fourth term accounts for redistribution of oscillators between branches in the range $[\psi_3^b, \psi_4^b]$ (Fig. 1(b)). In the last term the interval $\mathcal{X} = (-\infty, z + Y_{min}) \bigcup (z + Y_{max}, \infty)$ is the domain of frequencies where the oscillators are not locked.

Now, using the integrals (15), one can calculate the absolute values of the complex order parameters $R_{1,2}$ and the frequency Ω as functions of introduced parameters R, u, v, z:

$$R_{1,2}(\mathbf{P}) = RF_{1,2}(\mathbf{P}), \qquad \Omega(\mathbf{P}) = Rz. \tag{16}$$

Then, from relations (8), (10) and (16) it follows that:

$$\begin{aligned} \varepsilon(\mathbf{P}) &= \frac{\sin u}{F_1(\mathbf{P})}, \qquad \gamma(\mathbf{P}) = \frac{\cos u}{F_2(\mathbf{P})}, \\ \beta_1(\mathbf{P}) &= Q_1(\mathbf{P}), \qquad \beta_2(\mathbf{P}) = Q_2(\mathbf{P}) - v. \end{aligned} \tag{17}$$

All together Eqs. (16) and (17) determine the stationary amplitudes of the order parameters $R_{1,2}$ and the frequency of their rotation Ω in dependence on model parameters $\varepsilon, \gamma, \beta_{1,2}$ in an analytic, albeit parametric form. The parameters $\mathbf{P}$ uniquely define the distribution function $\rho(\psi|x, \mathbf{P})$, with a given indicator function S. This yields uniquely defined values of $R_{1,2}$. Therefore, a certain choice of parameters $\mathbf{P}$ and function S yields the values of $R_{1,2}, \varepsilon, \gamma, \beta_{1,2}$ and Ω. On the other hand, the order parameters and the oscillating frequency as functions of original system parameters $\varepsilon, \gamma, \beta_{1,2}$ can be multi-valued. Note that this solution fully accounts to multi-branch entrainment, due to presence of the indicator function S. Arbitrariness of this functions means that there is a huge multiplicity of microstates.

We stress, that in the solutions ((16), (17)) parameters R, u, v, z and the indicator function are *independent*, while the order parameters $R_{1,2}$ and the coupling parameters $\varepsilon, \gamma, \beta_{1,2}$ are functions of them. If, on the other hand, one wants to fix the coupling parameters, then one should adjust some of the parameters R, u, v, z and the indicator function, which will be now not independent. This is a standard procedure in a parametric representation of a solution.

4. Symmetric bi-harmonic coupling function

Here we consider the simplest case where $\beta_1 = \beta_2 = 0$, what corresponds to a symmetric coupling function $\Gamma(x) = \varepsilon \sin(x) + \gamma \sin(2x)$.

4.1. General solution of self-consistent equations

Symmetry of the coupling function allows us to perform the self-consistent approach in the special case $z = v = 0$ (see however Section 4.7 for a more general situation). First we will simplify equations (Eqs. (15)–(17)) taking into account the relation $z = v = 0$.

A typical form of function $y(u, v = 0, \psi)$ is presented in Fig. 1(d). For $v = 0$, the critical value $u = \pm\arctan(2)$ separates double-well and single-well shapes of function $y(u, 0, \psi)$. If $|\tan(u)| < 2$, the function $y(u, 0, \psi)$ contains two stable branches Ψ_1 and Ψ_2 (see Fig. 1(d)), otherwise only one branch Ψ_1 exists as shown in Fig. 1(c). The stable branches Ψ_1 and Ψ_2 (if the latter exists) are always centered in the intervals

$$\Psi_1 : [-\psi_1, +\psi_1] \quad \text{and} \quad \Psi_2 : [\pi - \psi_2, \pi + \psi_2],$$

where the values $\psi_{1,2}$ can be calculated explicitly:

$$\psi_{1,2} = \arccos\left(\frac{\mp \sin u + \sqrt{\sin^2 u + 32\cos^2 u}}{8\cos u}\right).$$

Moreover, the branches $\Psi_{1,2}$ are symmetric (see Fig. 1(d)):

$$\begin{aligned} y(u, 0, \psi) &= -y(u, 0, -\psi), \\ y(u, 0, \pi + \psi) &= -y(u, 0, \pi - \psi). \end{aligned} \tag{18}$$

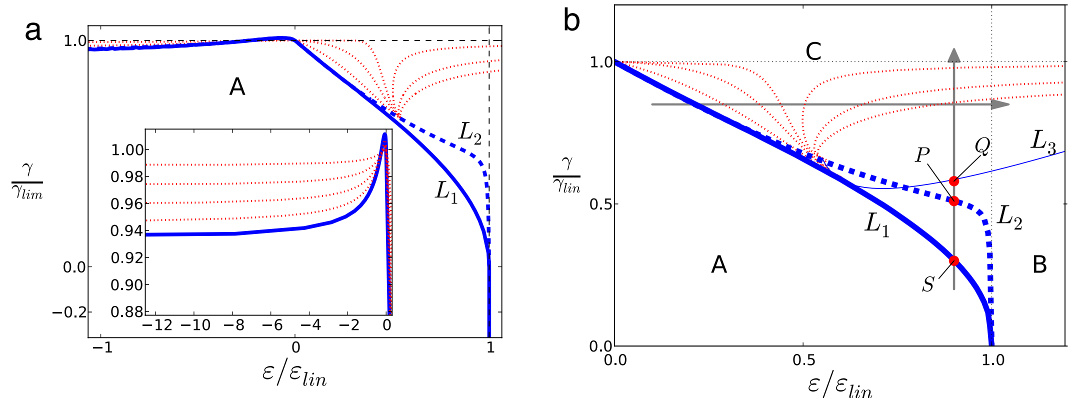

Fig. 2. (a) Diagram of different synchronous states in dependence on parameters (ε, γ), resulting from the analytical solution Eqs. (19) and (20). Bold (blue) line L_1: border of synchronous states, inside area A there is only the incoherent solution; between the lines L_1 and L_2 (bold dashed (blue) line) there are two solutions (stable and unstable) with non-zero $R_{1,2}$ and at the line L_2 the unstable branch touches zero (see region between points S and P in Fig. 3(a)). Dotted (red) lines: onset of synchrony for $\sigma = 0.2, 0.4, 0.5, 0.6, 0.8, 1$ (from left to right). Inset shows the domain of large in absolute value negative $\varepsilon < 0$ in more details (with the same axes definitions). (b) The same as in Fig. 2(a) but in the area $\varepsilon, \gamma > 0$. An additional line L_3 is drawn from the condition $\tan u = 2$, dividing domains B (single synchronous state) and C (multiple synchronous states). Above L_3 multiplicity of synchronous states due to multi-branch entrainment occurs (beyond point Q in Fig. 3(a)).

Taking all this into account, the relation (15) can be radically simplified:

$$F_m(R,u)e^{iQ_m(R,u)} = \int_{-\psi_1}^{\psi_1} d\psi e^{im\psi}(1-S(y))g(R(y))\frac{\partial y}{\partial \psi} + \int_{\pi-\psi_2}^{\pi+\psi_2} d\psi e^{im\psi}(S(y))g(R(y))\frac{\partial y}{\partial \psi} + \int_{|x|>x_1}\int_0^{2\pi} dxd\psi \frac{C(x)e^{im\psi}}{|x-z-y|}. \tag{19}$$

Similar to Eq. (15), the first term in Eq. (19) represents integral over the stable branch Ψ_1 in the range $[-\psi_1, \psi_1]$. We assume that the indicator function $S(y) = 0$ everywhere outside interval $[-\psi_1^b, \psi_1^b]$ (range of microscopic bistability, see Fig. 1(d)). The second term represents contribution of the oscillators on the second branch Ψ_2 in the range $[\pi - \psi_2, \pi + \psi_2]$ and the last term accounts for the contribution of the unlocked oscillators. If the functions $S(x)$ and $g(x)$ are even, then it is easy to see that the imaginary part in all of the integrals in (19) vanishes (recall that $y(u, 0, \psi)$ is odd). Thus, for any $S(x) = S(-x)$ and $g(x) = g(-x)$ we obtain $Q_{1,2}(R, u) = 0$ and automatically $\beta_{1,2} = 0$. (See Section 4.7 below for discussion of an asymmetric indicator function S.)

In summary, for the case $z = v = 0$ and even $S(x)$, $g(x)$ we have $\Omega = \beta_{1,2} = 0$ and the following expressions for the parameters ε, γ and real order parameters $R_{1,2}$ as functions of two introduced parameters R, u:

$$R_{1,2}(R,u) = RF_{1,2}(R,u), \qquad \varepsilon(R,u) = \frac{\sin u}{F_1(R,u)}, \qquad \gamma(R,u) = \frac{\cos u}{F_2(R,u)}. \tag{20}$$

4.2. Stability of the incoherent state

Before proceeding with presentation of the main results we recall that an issue of linear stability of the incoherent state (with uniform distribution of phases) was a milestone in almost all preceding mathematical studies [37,24,25,27] of Kuramoto-type models. This analysis of the partial differential equation for the density distribution function revealed the following stability properties of the incoherent state [37,24,25,27]: (i) the continuous part of the spectrum always lies on the imaginary axis; (ii) when one of the couplings exceeds certain threshold $\varepsilon > \varepsilon_{lin}$ or $\gamma > \gamma_{lin}$, in the discrete spectrum appears an eigenvalue with a positive real part revealing instability of the asynchronous state. In the linear theory, the modes of the perturbation corresponding to the harmonics of the coupling are independent on each other, and one gets $\varepsilon_{lin} = \gamma_{lin} = \frac{2}{\pi g(0)}$. Below in this paper we use a Gaussian distribution of frequencies $g(\omega) = (2\pi)^{-1/2}\exp(-\omega^2/2)$, thus $\varepsilon_{lin} = \gamma_{lin} = 2\sqrt{\frac{2}{\pi}}$. In presentation of the results, we will always normalize the values of the coupling parameters ε, γ by the linear stability thresholds.

4.3. Diagram of synchronous states

In Fig. 2 we illustrate the diagram of the states on the plane of parameters (ε, γ), and in Fig. 3 some cuts of it, for the simplest case, where the indicator function $S(\omega) = \sigma$ is a constant. This diagram is obtained by application of analytic formulas (20).

We start the description with an even simpler case $\sigma = 0$ (so that all the phases are on one stable branch). Setting in (19), (20) $R = 0^+$ and varying u, we find a curve on the plane of parameters (ε, γ) where a solution with going to zero order parameters $R_{1,2}$ exists (line L_2 in Fig. 2, see Section 4.8 below for the details of calculation of this line), possibly coexisting with another solutions. In the plane (ε, γ) also exists the curve L_1, which corresponds to the line of a "saddle–node bifurcation" where two branches of coherent solutions first appear (point S in Fig. 3(a)). This means that nontrivial solutions $R_{1,2}(\varepsilon, \gamma) > 0$ appear via a first-order transition, as the coupling strengths (ε, γ) increase (Fig. 3(a)); exception are the pure cases $\varepsilon = 0$ and $\gamma = 0$, where L_1 touches L_2 (see Section 4.8 below). The line L_1 splits the plane (ε, γ) in two different regions: in area A in Fig. 2(a, b) only incoherent solution of self-consistent equations exists, outside area A (regions B and C in Fig. 2(b)) synchronous solution(s) exist. Between curves L_1 and L_2 there are two solutions with $\sigma = 0$. We also show a curve L_3 corresponding to the parameter value $\tan u = 2$, which separates the two-branch (Fig. 1(a,d)) and the one-branch (Fig. 1(b)) situations (marked as C and B on panel Fig. 2(b) correspondingly).

Below L_3 there is a solution with $S(\omega) = 0$ only, above it, multiplicity due to arbitrariness of the indicator function $S(\omega)$ occurs. We depict also curves corresponding to synchronous solutions with $R_{1,2} = 0^+$ at several fixed values of σ (red curves in Fig. 2), to the right of these curves synchronous states with corresponding values of σ exist.

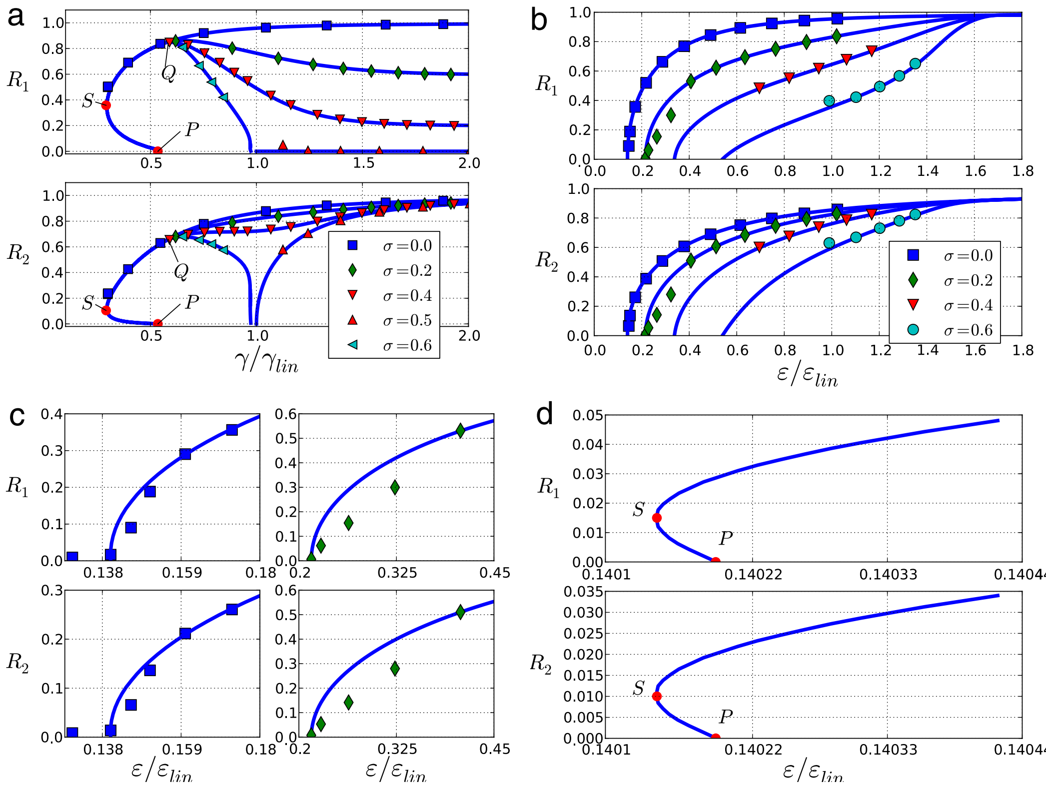

Fig. 3. (a) Dependence of the order parameters $R_{1,2}$ on coupling strength γ at fixed value of $\varepsilon = 0.9\varepsilon_{lin}$ (see also vertical arrow in Fig. 2(b)). Markers are results of direct simulation of a population of $N = 2 \cdot 10^4$ oscillators. Different curves correspond to different values of σ, as depicted on the panel. For $\gamma \lesssim 0.6\gamma_{lin}$ there is a unique synchrony state, for larger couplings multiplicity is observed. Point S denotes a "saddle–node bifurcation" at which coherent states appear (curve L_1 in Fig. 2). At point P the order parameters at the unstable branch of coherent solution vanish (curve L_2 in Fig. 2). Between points S and P a finite perturbation of the incoherent state is needed to come to a synchronous regime. Point Q, the onset of multiplicity, corresponds to curve L_3 in Fig. 2(b). (b) The same as in Fig. 3(a) but for $\gamma = 0.9\gamma_{lin}$, and varying ε (horizontal arrow in Fig. 2(b)). For $\varepsilon \gtrsim 1.6\varepsilon_{lin}$ the solution is unique, for smaller ε there are multiple states with different σ appearing at different critical couplings. (c) Detailed view of curves $R_{1,2}(\varepsilon)$ for $\sigma = 0$ (left panels) and $\sigma = 0.2$ (right panels). For both cases $\gamma = 0.9\gamma_{lin}$. Here markers denote averaged values of stationary order parameters of different independent numerical simulations (see text). (d) Enlargement of the curves $R_{1,2}(\varepsilon)$ ($\sigma = 0$, $\gamma = 0.9\gamma_{lin}$, panel(b)) for small values of order parameters, indicating a first-order type of the transition, hardly seen in panel (b). Thus in both cases (panels (a) and (b)) near the point P the dependence of $R_{1,2}$ on coupling constants ε and γ is linear with negative slope (see Section 4.8 for details).

We illustrate different synchronous regimes as functions of coupling parameters (ε, γ) in Fig. 3(a, b). Fig. 3(a) shows dependence of synchronous states on the coupling parameter γ for fixed $\varepsilon = 0.9\varepsilon_{\text{lin}}$ (vertical arrow in Fig. 2(b)). As it has been mentioned above, two branches of coherent solutions arise at point S. With increase of γ, the lower branch merges with the incoherent solution at point P. The upper branch is unique until the border of multiplicity $\tan u = 2$ (point Q) is crossed. Multiple solutions exist for all larger values of γ.

A special symmetric solution appears at the linear threshold $\gamma = \gamma_{lin}$. This regime contains only the second harmonic ($R_1 = 0$) and has symmetric redistribution of oscillators ($\sigma = 0.5$) between the two symmetric stable branches. This regime appears as a square root of supercriticality $R_2 \sim (\gamma - \gamma_c)^{\frac{1}{2}}$ (see the branch of R_2 starting at $\gamma/\gamma_{lin} = 1$ for $\sigma = 0.5$ in Fig. 3(a)) and corresponds to the bifurcation from the asynchronous state as described in [24,25].

In Fig. 3(b) the order parameters are shown as functions of ε for fixed $\gamma = 0.9\gamma_{lin}$ (horizontal arrow in Fig. 2(b)). As for parameters almost everywhere here we are in the region of multiplicity, the synchrony arises at different values of ε for different σ. Immediately beyond the threshold (which corresponds to $\sigma = 0$) multiple synchrony states with $\sigma > 0$ are possible (as here $\tan u < 2$). With further increase of ε, when the line L_3 is crossed (at large values of ε not shown in Fig. 2(b)), multiplicity disappears.

In contrast to Fig. 3(a), the first synchronous solution $\sigma = 0$ in Fig. 3(b) looks like arising via a second-order phase transition. However a detailed analysis of the situation in Fig. 3(d) shows that this is not the case (as was erroneously stated in [20]). With decrease of parameter u to zero (decrease of ε), lines L_1 and L_2 come close to each other but they merge only at the point $u = 0$ which corresponds to the pure second-harmonics Kuramoto model ($\varepsilon = 0$). In the Section 4.8 below, using a combination of the self-consistent approach and a perturbative analysis, we will show that at L_2 the dependence of $R_{1,2}$ on coupling strengths ε and γ is linear with a negative slope, everywhere except at singular points $u = 0$ and $u = \pi/2$ which correspond to the pure cases of second-harmonic and first-harmonic Kuramoto models, respectively.

4.4. Stability properties

Unfortunately, we cannot perform analytically, and even numerically, a thorough stability analysis of the constructed solutions. The only analytic results we can rely on, are outlined in Section 4.2. Stability calculations of the asynchronous state $R_{1,2} = 0$ yield instability for $\varepsilon > \varepsilon_{\text{lin}}$ or $\gamma > \gamma_{\text{lin}}$, and neutral stability with a continuous spectrum for $\varepsilon < \varepsilon_{\text{lin}}$, $\gamma < \gamma_{\text{lin}}$ [37,24,25,27]. This conclusion can be easily reproduced numerically. However, we could not study stability of self-consistent solutions in the same manner, because these solutions have a singular component (delta-function in Eqs. (13) and (14)).

Therefore, we checked for stability via direct numerical simulation of large ensembles (see also [21]). The found solutions follow the theoretically predicted curves as shown by markers in

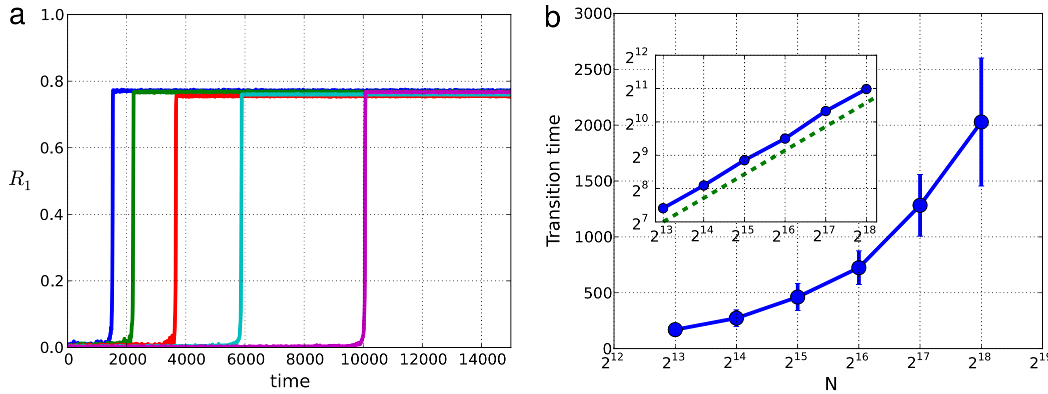

Fig. 4. (a) Examples of time evolution of the order parameter R_1 in direct simulations of an ensemble (1) for $\gamma = 0.85\gamma_{lin}$, $\varepsilon = 0.6\varepsilon_{lin}$ and different N (from left to right, $N = 5\cdot 10^4, 10^5, 2\cdot 10^5, 5\cdot 10^5, 10^6$). (b) Averaged transition times from the incoherent state to a synchronous solution, in dependence on the ensemble size N for $\gamma = 0.85\gamma_{lin}$, $\varepsilon = 0.6\varepsilon_{lin}$. Error bars show standard deviations. Each point was obtained from a statistics of 128 different simulations. Inset shows the same plot in log–log scale. One can see a power law with exponent ≈ 0.72 (dashed line).

Fig. 3(a, b). However, the stability of states with small values of $R_{1,2}$ cannot be easily confirmed due to finite-size effects.

In order to study these finite-size effects in the vicinity of "bifurcation points", i.e. for small values of the order parameters, we performed additional simulations with large ensemble size $N = 2^{18} = 262144$. Two theoretical curves with $\sigma = 0$ and $\sigma = 0.2$ for $\gamma = 0.9\gamma_{lin}$ (Fig. 3(b)) have been tested for stability. In each simulation we independently generated random distribution of frequencies for $N = 262144$ oscillators and prepared initial conditions according to the distribution function, obtained from our self-consistent analysis at given parameters. As a result, Fig. 3(c) shows the averaged values of $R_{1,2}$ (obtained from the numerical simulation of more than 32 independent runs for each point). One can see that the markers are slightly below the curves, indicating that on an average synchronization is weaker than the analytically predicted level. Nevertheless, certain level of coherence is always present and it is reasonably in agreement with analytically predicted curves.

Next, we simulated the linearly neutrally stable asynchronous state, in the region beyond the curve L_2, where also synchronous solutions exist. In simulations this state appears to be only *metastable*. After a transient, which becomes longer for very large ensembles, the ensemble evolves abruptly to one of the synchronous states, we illustrate this in the Fig. 4(a). Remarkably, the averaged time that the system spends in the vicinity of incoherent metastable state grows as a power law of number of oscillators N (Fig. 4(b)).

Thus, although the curves in Fig. 3(b) look like a standard hysteretic transition, it is not the case: on line L_2 (at point P) the incoherent steady state does not become linearly unstable, instead it remains linearly neutrally stable in the thermodynamic limit, but is metastable due to finite-size effects. This neutral stability/metastability allows also synchronous states to appear with arbitrary small amplitudes $R_{1,2}$ (see on Fig. 2(a, b) curve L_2 and corresponding curves for different values of σ, which occupy the whole region on this diagram, and also Fig. 3(b)). Therefore, the points in Fig. 3(b) where $R_{1,2}$ vanish, do not correspond to a usual bifurcation from an equilibrium, and cannot be described as the points where the incoherent state becomes linearly unstable. While this issue requires further investigation, we attribute it to the singularity of the appearing states: as one can see from Eqs. (13), (14), the density includes a combination of delta-functions for any small $R_{1,2}$, similar to the Van Kampen modes in plasmas [38]. On the other hand, in the stability analysis [24,25] one operates with modes which are non-singular.

4.5. Illustration of multi-branch entrainment states

Here we discuss the issue of multiplicity and illustrate different multi-branch entrainment states [29,30]. As mentioned above, in the thermodynamic limit any indicator function $S(x)$ is admissible. Thus for fixed parameters ε, γ, a macro-state with given order parameters $\varepsilon, \gamma, R_{1,2}$ contains many micro-states with different redistributions between the stable branches. In Fig. 5 we show several multi-branch states obtained from different initial conditions for a certain choice of coupling parameters. In Fig. 5(a)–(c), we have chosen a two-cluster state as an initial condition. Phases were set to $\varphi_k = 0$ or to $\varphi_k = \pi$ $(k = 1, \ldots, N)$ with probabilities $1 - \sigma$ and σ, correspondingly.

So far, we considered only constant indicator function $S(\omega) = \sigma$, so that the redistribution of oscillators between the branches was independent of their natural frequencies. However, in the self-consistent approach the function $S(\omega)$ appears only in the integrals (15), therefore it is arbitrary integrable function which can be extremely non-smooth. Fig. 5(d) shows the example of wildly varying function $S(\omega)$, what corresponds to practically random redistribution of oscillators at different internal frequencies ω. Such a state was obtained by splitting initial values of phases into two clusters where $\varphi_k = 0$ or $\varphi_k = \pi$ $(k = 1, \ldots, N)$ with different probabilities for different internal frequencies ω.

If both branches are occupied, one observes a two-hump distribution of locked phases which can be also interpreted as a two-cluster state (cf. [35]).

In fact, we can easily estimate the degree of the multiplicity. We can view the locked oscillators in the bistability range as "uncoupled spins". Assuming for simplicity that the phases of two branches differ by π, we conclude that the order parameter R_2 does not depend on the "spin orientation", i.e. on which branch they are sitting, while R_1 can be interpreted as a "magnetization". Then finding the number of different micro-states at prescribed values of the order parameters reduces to a textbook problem of calculating the entropy

$$\mathcal{S}(R_1) = N_{\text{bist}}\left[-\left(\frac{1-R_1}{2}\right)\ln\left(\frac{1-R_1}{2}\right) - \left(\frac{1+R_1}{2}\right)\ln\left(\frac{1+R_1}{2}\right)\right] \quad (21)$$

under condition of a constant magnetization, for N_{bist} non-interacting spins (the latter is the number of locked oscillators in the range of bistability; it is less than N but is a macroscopic quantity for $R_{1,2}$ not too small). Correspondingly, the number of micro-states grows exponentially with the number of locked

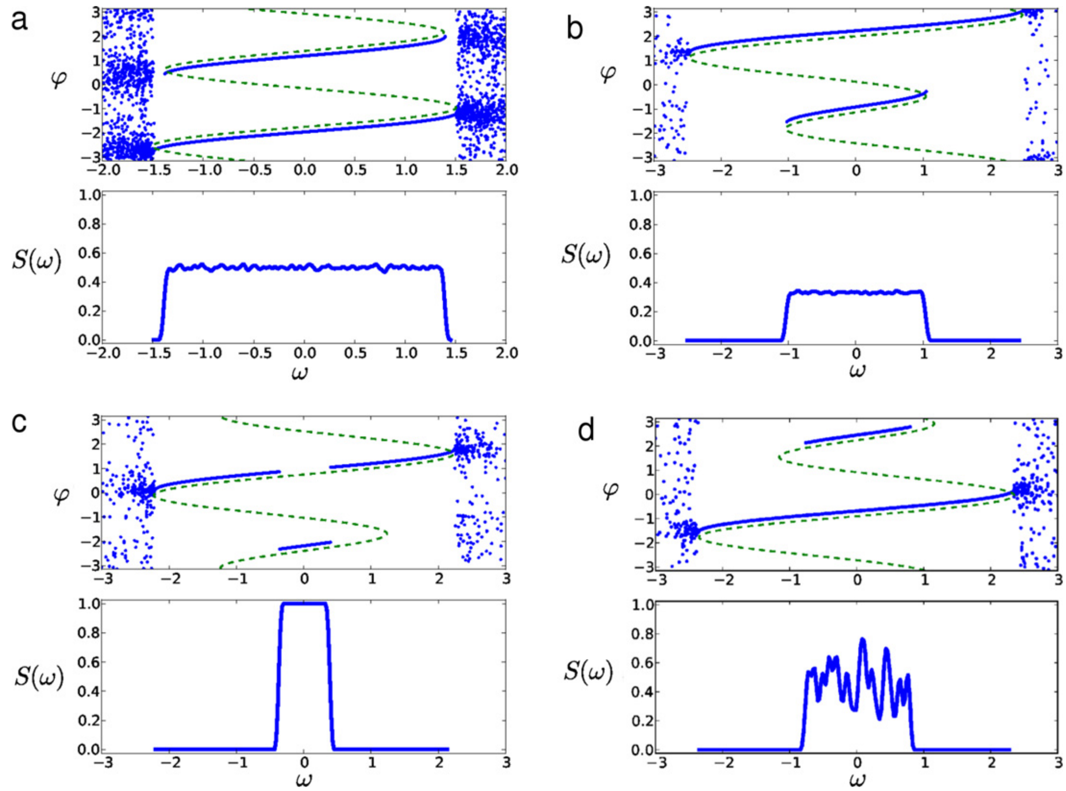

Fig. 5. Illustration of multiplicity of states ($\varepsilon = \gamma = 1.25\varepsilon_{\text{lin}}$, $N = 2 \cdot 10^4$). In all cases one can see two stable branches of locked phases and the corresponding coarse-grained indicator function $S(\omega)$.

oscillators $\sim e^{\mathcal{S}(R_1)}$ (cf. [30]). We stress here that while the entropy (21) gives the number of micro-states at given macroscopic order parameters, it does not define any relative stability of the macroscopic states, as the evolution of oscillators is dissipative and not a Hamiltonian evolution needed for application of microcanonical arguments. In fact, the relative size of the basins of attractions for different macro-states may not follow Eq. (21).

4.6. Competition of the coupling terms

A non-trivial consequence of the multi-branch entrainment occurs in the region of negative ε. When $\varepsilon < 0$, the coupling due to the first mode in the coupling function is repulsive (or desynchronizing); it tends to stabilize the incoherent state and to destroy synchrony. With the second harmonic in coupling function, one might expect that the repulsion for large negative ε should be compensated by a strong attractive second-harmonic coupling with large positive γ, for synchronization in the system to occur. However, following the curve L_1 in Fig. 2(a) one can see that the critical value of γ *decreases* and tends to some constant value below γ_{lin} as $\varepsilon \to -\infty$. This means that the effect of very strong repulsive coupling via the first harmonics can be compensated by a relatively weak synchronizing force $\sim \gamma$. Fig. 6(a) shows dependences $R_{1,2}(\gamma)$ at $\varepsilon = -9.29\varepsilon_{lin}$. Remarkably, the presented solutions are characterized by rather low values of R_1. The plots of $\phi(\omega)$ in Fig. 6(b, c) shed light onto this effect. In the region $\varepsilon > 0$ the solutions appearing on the line L_1 have simple structure of single-branch entrainment states (Fig. 6(b)). On the contrary, in the region of repulsing first-harmonic coupling $\varepsilon < 0$, the appearing solutions represent two-cluster states with indicator function $S = 1$, like in Fig. 6(c). The oscillators are distributed among the branches in such a way that the value of R_1 is minimal, so that effective repulsive force εR_1 (see Eq. (4)) is sufficiently weak.

4.7. Non-symmetric solutions

Until now we considered the cases where the functions $S(x)$ (indicator function) and $g(x)$ (distribution of frequencies) were even $S(x) = S(-x)$, $g(x) = g(-x)$. Such symmetric indicator and frequency distribution functions yield solutions with $\beta_{1,2} = 0$ and $\Omega = 0$ at zero values of parameters $z = v = 0$ in the self-consistent equations ((15)–(17)). However in the general case of non-even $S(x)$ or $g(x)$ zero values of $\beta_{1,2}$ correspond to certain non-zero z and v. For example, asymmetric redistribution of oscillators between stable branches (a non-even indicator function $S(x) \neq S(-x)$) gives rise to a non-zero frequency shift $\Omega = Rz \neq 0$ even in the case of $\beta_{1,2} = 0$ and symmetric distribution of frequencies g. The example is presented in Fig. 7 where we use $S(x) = \sigma$ for $x < (x_1^b + x_2^b)/2$ (see Fig. 1(b)) and $S(x) = 0$ otherwise.

4.8. Perturbative analysis near critical points

In this section we combine the self-consistent approach ((19), (20)) with a perturbative analysis, to derive the scaling law of macroscopic order parameters in the vicinity of bifurcation line L_2 (Fig. 2) where coherent solution appears. The idea is to consider ((19), (20)) in the limit $R \to 0$ and to find dependence of $R_{1,2}$ on criticalities $(\varepsilon - \varepsilon_c)$ and $(\gamma - \gamma_c)$ in this limit of vanishing order parameters. For simplicity of presentation we will assume below $S(x) = 0$ (all oscillators are on the same branch and ε_c, γ_c are on the curve L_2) and shortly discuss other possibilities at the end of this section. In this case (19) reads

$$F_m = \int_0^{2\pi} d\psi \cos m\psi \, g(Ry)\frac{\partial y}{\partial \psi} + \int_0^{2\pi} d\psi \int_{|x|>x_1}^{\pm\infty} dx \frac{g(Rx)C'(x)\cos(m\psi)}{|x - y(u,\psi)|} \equiv A_m(R,u) + B_m(R,u), \quad m = 1, 2.$$

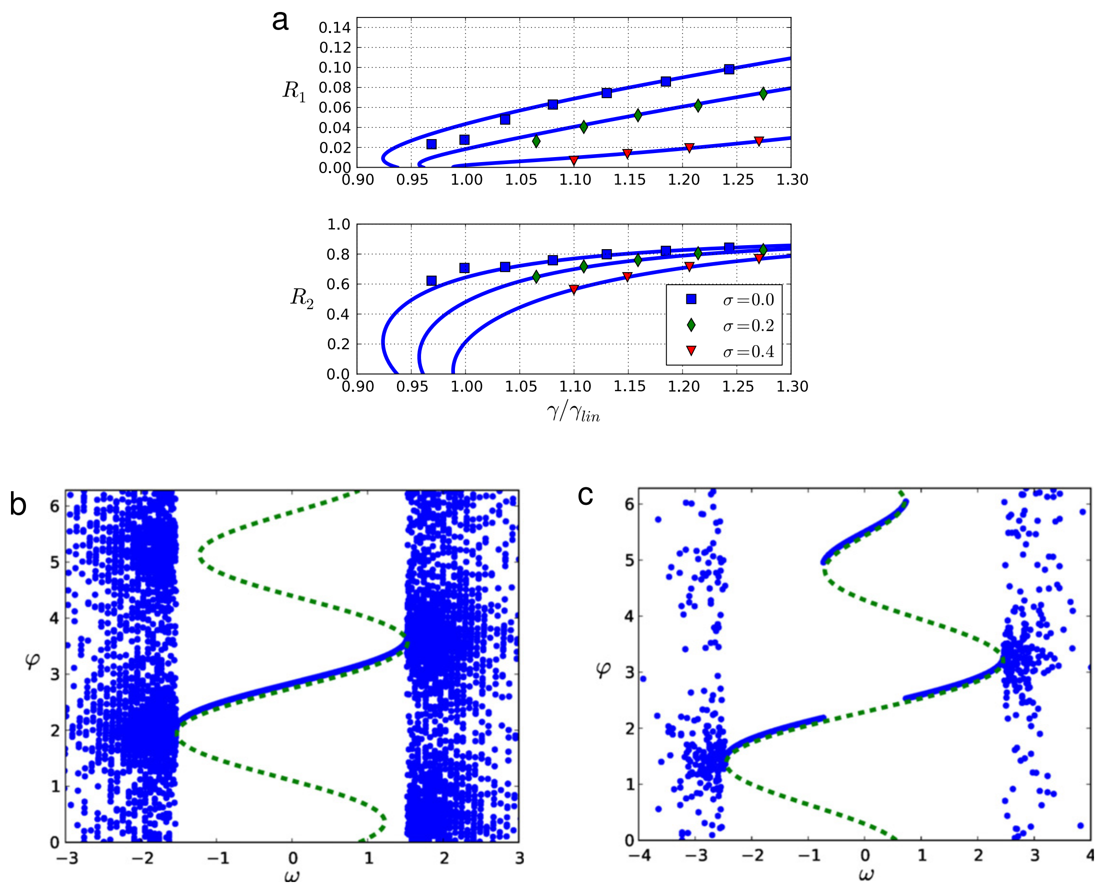

Fig. 6. (a) Dependence of order parameters $R_{1,2}$ on coupling strength γ at $\varepsilon = -9.29\gamma_{lin}$. (b, c) Phases of oscillators versus internal frequencies. For both cases $\gamma = 1.18\gamma_{lin}$. In panel (b) $\varepsilon = 0.16\varepsilon_{lin}$, in panel (c) $\varepsilon = -9.29\varepsilon_{lin}$. Markers in panel (a) are result of direct simulation for $N = 2 \times 10^4$.

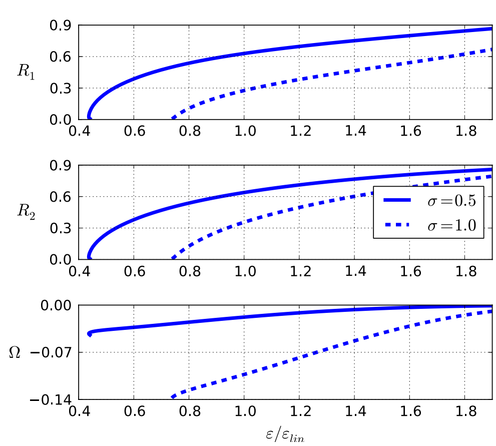

Fig. 7. Dependence of the order parameters $R_{1,2}$ and their frequency Ω on coupling strength ε at $\gamma = 0.9\gamma_{lin}$ and $\beta_{1,2} = 0$ for non-even indicator function: $S(x) = \sigma$ for $x < (x_1^b + x_2^b)/2$ (see Fig. 1(b)) and $S(x) = 0$ otherwise.

(Here C' is the normalization constant.) Because $g(x)$ is a symmetric unimodal density, its expansion for small arguments reads $g(x) = g(0) - G_2x^2 + \cdots$. Suppose that $R \ll 1$, then the first term in equation for F_m can be represented using this series for g as follows:

$$A_m = \int_0^{2\pi} d\psi \cos m\psi \,(g(0) - G_2R^2y^2)\frac{\partial y}{\partial \psi} = A_{m0} - A_{m2}R^2. \quad (22)$$

For calculation of the second term B_m we first compute

$$\Phi_m(x) = \frac{\int_0^{2\pi} \frac{d\psi \cos(m\psi)}{|x-y(u,\psi)|}}{\int_0^{2\pi} \frac{d\psi}{|x-y(u,\psi)|}}.$$

With notation $z = 1/x$ we get

$$\Phi_m(z) = \frac{\int_0^{2\pi} \frac{d\psi \cos(m\psi)}{|1-zy(u,\psi)|}}{\int_0^{2\pi} \frac{d\psi}{|1-zy(u,\psi)|}} = \frac{\int_0^{2\pi} d\psi \cos(m\psi)[1 + zy(u,\psi) + z^2y^2(u,\psi) + \cdots]}{\int_0^{2\pi} d\psi[1 + zy(u,\psi) + z^2y^2(u,\psi) + \cdots]}.$$

Substituting here expression for y we get

$$\Phi_1(z) = \frac{z^2\pi \sin u \cos u}{2\pi + z^2\pi} \approx z^2\frac{1}{2}\sin u \cos u = z^2\Phi_{12},$$

$$\Phi_2(z) = \frac{z^2\pi(-\sin^2 u/2)}{2\pi + z^2\pi} \approx -z^2\frac{1}{4}\sin^2 u = z^2\Phi_{22},$$

or in the old notation

$$\Phi_1(x) = x^{-2}\Phi_{12}, \qquad \Phi_2(x) = x^{-2}\Phi_{22},$$
$$\Phi_{12} = \frac{\sin u \cos u}{2}, \qquad \Phi_{22} = -\frac{\sin^2 u}{4}. \quad (23)$$

The last expressions are valid for $x \gg 1$. For small x, Φ_m are bounded from above $\Phi_m(x) \le \bar{\Phi}_m$.

Now we can rewrite the integrals in the expression for B_m as

$$B_m = \int_{|x|>x_1}^{\pm\infty} dx g(Rx)\Phi_m(x) = 2\int_{x_1}^{\infty} dx g(Rx)\Phi_m(x)$$

$$= 2\int_{x_1}^{\infty} dx g(0)\Phi_m(x) + 2\int_{x_1}^{\infty} dx[g(Rx) - g(0)]\Phi_m(x)$$
$$\equiv B_{m0} - \tilde{B}_m.$$

To calculate the last term, we divide the integration range into two subintervals

$$\begin{aligned}\tilde{B}_m &= 2\int_{x_1}^{\infty} dx[g(0) - g(Rx)]\Phi_m(x)\\ &= 2\int_{x_1}^{R^{-1/6}} dx[g(0) - g(Rx)]\Phi_m(x)\\ &\quad + 2\int_{R^{-1/6}}^{\infty} dx[g(0) - g(Rx)]\Phi_m(x).\end{aligned}$$

In the first interval we use the upper bound for Φ_m, and because here $Rx \ll 1$, we use the expansion $g(x) = g(0) - G_2x^2$:

$$\begin{aligned}&2\int_{x_1}^{R^{-1/6}} dx[g(0) - g(Rx)]\Phi_m(x) < 2\bar{\Phi}_m G_2 R^2 \int_{x_1}^{R^{-1/6}} x^2 dx\\ &= 2/3\bar{\Phi}_m G_2 R^2 (R^{-1/2} - x_1^3) = \mathcal{O}(R^{3/2}).\end{aligned}$$

In the second integral, because $x \gg 1$, we use the expansion (23) for $\Phi_m(x)$

$$\begin{aligned}&2\int_{R^{-1/6}}^{\infty} dx[g(0) - g(Rx)]\Phi_m(x)\\ &= 2\Phi_{m2}\int_{R^{-1/6}}^{\infty} dx[g(0) - g(Rx)]x^{-2}\\ &= 2\Phi_{m2}R\int_{R^{5/6}}^{\infty} dz[g(0) - g(z)]z^{-2}\\ &= 2\Phi_{m2}R\int_{0}^{\infty} dz[g(0) - g(z)]z^{-2}\\ &\quad - 2\Phi_{m2}R\int_{0}^{R^{5/6}} dz[g(0) - g(z)]z^{-2}\\ &\approx \Phi_{m2}R\Gamma - 2\Phi_{m2}RG_2\int_0^{R^{5/6}} dz \approx \Phi_{m2}RQ\end{aligned}$$

where

$$Q = 2\int_0^{\infty} dz[g(0) - g(z)]z^{-2}$$

characterizes the frequency distribution, and we neglected terms having higher orders in R. Summing together we get

$$B_m = B_{m0} - RQ\Phi_{m2}.$$

Thus, in the leading order, we obtain the following expressions for the functions F_m:

$$F_m(R, u) = A_{m0} + B_{m0} - RQ\Phi_{m2} = F_{m0}(u) - RQ\Phi_{m2}(u). \qquad (24)$$

Here we can immediately identify cases where the expansion (24) is not sufficient corresponding to situations where $\Phi_{m2} = 0$. For $u = 0$ we have $\Phi_{12} = \Phi_{22} = 0$; according to Eq. (20) this corresponds to $\varepsilon = 0$, i.e. to pure second harmonic coupling. For $u = \pi/2$ only one coefficient vanishes $\Phi_{12} = 0$, this corresponds to the standard Kuramoto model with $\gamma = 0$. In both cases the dependences of the order parameters on the coupling constants follow the square-root law $R_1 \sim (\varepsilon - \varepsilon_{\text{lin}})^{1/2}$, $R_2 \sim (\gamma - \gamma_{\text{lin}})^{1/2}$ [13].

Using general expression (24) we can find how the order parameters depend on the coupling constants for any crossing of the critical curve. Suppose we consider a critical point ε_c, γ_c corresponding to u_c, and we choose some direction q of crossing the criticality, so that $u = u_c + qR$. Then

$$\begin{aligned}\varepsilon &= \frac{\sin u}{F_{10}(u) - R\Gamma\Phi_{12}(u)} = \frac{\sin u_c + \cos u_c qR}{F_{10}(u_c) + (F_{10}'q - \Gamma\Phi_{12}(u_c))R}\\ &= \frac{\sin u_c}{F_{10}(u_c)} + R\left[q\frac{\cos u_c}{F_{10}(u_c)} - \frac{\sin u_c(F_{10}'q - \Gamma\Phi_{12}(u_c))}{F_{10}^2(u_c)}\right]\\ &= \varepsilon_c + \varepsilon_1(q)R,\\ \gamma &= \frac{\cos u}{F_{20}(u) - R\Gamma\Phi_{22}(u)} = \frac{\cos u_c - \sin u_c qR}{F_{20}(u_c) + (F_{20}'q - \Gamma\Phi_{22}(u_c))R}\\ &= \frac{\cos u_c}{F_{20}(u_c)} + R\left[q\frac{-\sin u_c}{F_{20}(u_c)} - \frac{\cos u_c(F_{20}'q - \Gamma\Phi_{22}(u_c))}{F_{20}^2(u_c)}\right]\\ &= \gamma_c + \gamma_1(q)R.\end{aligned}$$

This yields

$$R_m = \frac{F_{m0}(u_c)}{\varepsilon_1(q)}(\varepsilon - \varepsilon_c) = \frac{F_{m0}(u_c)}{\gamma_1(q)}(\gamma - \gamma_c). \qquad (25)$$

Choosing parameter $q = q_0$ in such a way that $\gamma_1(q_0) = 0$ we have:

$$R_m = \kappa_m^{\varepsilon}(\varepsilon - \varepsilon_c), \qquad \gamma \equiv \gamma_c, \qquad (26)$$

and $\gamma_1(q_0) = 0$ implies that:

$$q_0 = \frac{\cos u_c \Gamma\Phi_{22}(u_c)}{\sin u_c F_{20}(u_c) + \cos u_c \frac{\partial F_{20}}{\partial q}}.$$

The same for $\varepsilon_1(q_1) = 0$:

$$R_m = \kappa_m^{\gamma}(\gamma - \gamma_c), \qquad \varepsilon \equiv \varepsilon_c \qquad (27)$$

with

$$q_1 = \frac{\sin u_c \Gamma\Phi_{12}(u_c)}{\sin u_c \frac{\partial F_{10}(u_c)}{\partial q} - F_{10}(u_c)\cos u_c}.$$

Here we denote

$$\kappa_m^{\varepsilon}(u_c) = \frac{F_{m0}(u_c)}{\varepsilon_1(q_0)}, \qquad \kappa_m^{\gamma}(u_c) = \frac{F_{m0}(u_c)}{\gamma_1(q_1)}. \qquad (28)$$

Eqs. (25)–(27) show that generally the order parameters $R_{1,2}$ scale *linearly* at the “bifurcation points”, in contradistinction to the situations $\varepsilon = 0$ and $\gamma = 0$, see also [39] for the first discovery of this scaling.

For the Gaussian distribution of frequencies $g(\omega) = \frac{1}{\sqrt{2\pi}}e^{-\frac{x^2}{2}}$ the constant Q can be evaluated explicitly and it is equal to one. In the latter case calculations of (28) show (Fig. 8) that $\kappa_{1,2}^{\varepsilon,\gamma}(u_c)$ are finite and non-zero everywhere except for the above mentioned singular points $u_c = 0$ and $u_c = \pi/2$, which correspond to the one-harmonic Kuramoto model where the transition has a continuous second-order type form.

According to numerical simulations of finite-size ensembles (Fig. 3), the appearing solutions at the line L_2 are unstable and they are not observable in an actual numerical simulation of the network. However, the linear scaling of the self-consistent order parameters (25) described above may shed light on the nature of the transition happening at line L_2. This is a nontrivial “bifurcation”, as the linear stability property of the trivial state $R_{1,2} = 0$ do not change. Analysis of this transition from the point of view of bifurcation theory should be a subject of further studies.

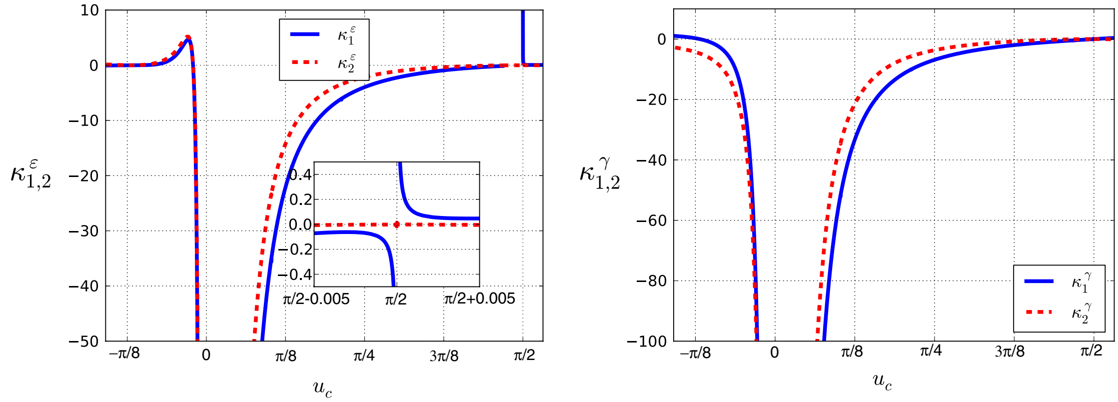

Fig. 8. Dependences of $\kappa^{\varepsilon,\gamma}_{1,2}$ on u_c (Eq. (28)).

5. Asymmetric coupling function

In this section we present several examples of application of our general theory for calculation of uniformly rotating synchronous states for the case of non zero phase shifts $\beta_{1,2}$ in the coupling function, see Eqs. (16) and (17). Here the number of control parameters $(\varepsilon, \gamma, \beta_1, \beta_2)$ is large, thus we do not perform a comprehensive analysis, but just illustrate applicability of the method.

The main general feature at non-zero phase shifts β_1, β_2 is a general appearance of the frequency shift Ω. Thus mean fields rotate with the frequency different from the mean frequency of the distribution $g(\omega)$. Fig. 9 shows dependences of the order parameters $R_{1,2}$ and of frequency Ω on coupling constants ε and γ, for fixed values of $\beta_{1,2} = \pi/8$ (Fig. 9(a)) and $\beta_{1,2} = \pi/4$ (Fig. 9(b)). These curves have been obtained from Eqs. (16) and (17) by adjusting free parameters **P** to achieve the given values of β_1, β_2.

Another interesting example is motivated by work of Hansel et al. [31]. In this paper the authors consider an ensemble of *identical* (with equal natural frequencies) phase oscillators with a bi-harmonic coupling function. At $\pi/3 < \beta_1 < \pi/2$, $\beta_2 = \pi$, $\varepsilon/\gamma = 4$ the authors describe slow periodic oscillations of the order parameters and show that these variations arise due to a closed heteroclinic cycle in the phase space of the model. Such an oscillating dynamics due to existence of heteroclinic cycles has been studied in details for relatively small ensembles in [40]. In order to model identical oscillators in our setup, one has to consider a delta-distribution of frequencies $g(\omega) = \delta(\omega)$. However, we have normalized the width of this distribution to one. Because normalization of frequencies is equivalent to normalization of time, in our approach the limit of identical oscillators corresponds to the limit $\varepsilon, \gamma \to \infty$ at a fixed width of the distribution $g(\omega)$. Therefore, we applied our method for the parameters $\beta_{1,2}$ as in [31], for very large values of the coupling constants.

Fig. 10(a) shows the solutions of Eqs. (15)–(17) at $\beta_1 = \pi/2.5$ $\beta_2 = \pi$ and $\varepsilon/\gamma = 4$, together with the results of direct numerical simulations of a large ensemble with $N = 2 \times 10^4$. At small values of coupling ($\varepsilon < 650$), the stationary state obtained from our self-consistent approach is reproduced by direct numerical simulations of (1) (the time series is shown in Fig. 10(b)). At larger values of the coupling, this stationary solution loses stability via (presumably) a supercritical Andronov–Hopf bifurcation at which slow oscillatory variations of the order parameters appear (Fig. 10(c)). This example shows that while we always can find a uniformly rotating solution with constant order parameters, this solution can be unstable in some parameter range, where a more complex dynamics establishes.

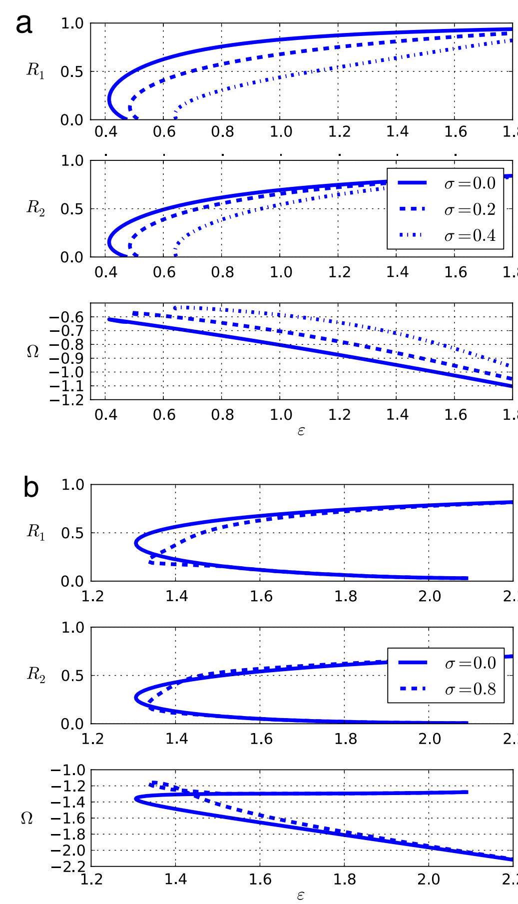

Fig. 9. Dependences of the order parameters $R_{1,2}$ and their frequency Ω on coupling strength ε at fixed values of $\beta_{1,2}$ and $\gamma = 1.5$. In the panel (a) $\beta_{1,2} = \pi/8$, in the panel (b) $\beta_{1,2} = \pi/4$. Here no normalization on the linear stability thresholds is performed.

6. Conclusion

In this paper we have described nontrivial synchronous states that appear in the Kuramoto model with a bi-harmonic coupling function. Here we summarize essential novel features compared to the standard Kuramoto setup.

1. Due to a possibility to have two stable branches of phase-locked oscillators, one observes a multi-branch locking with a multiplicity of micro-states [28,30]. On the macro-level, this multiplicity manifests itself as existence of a whole range

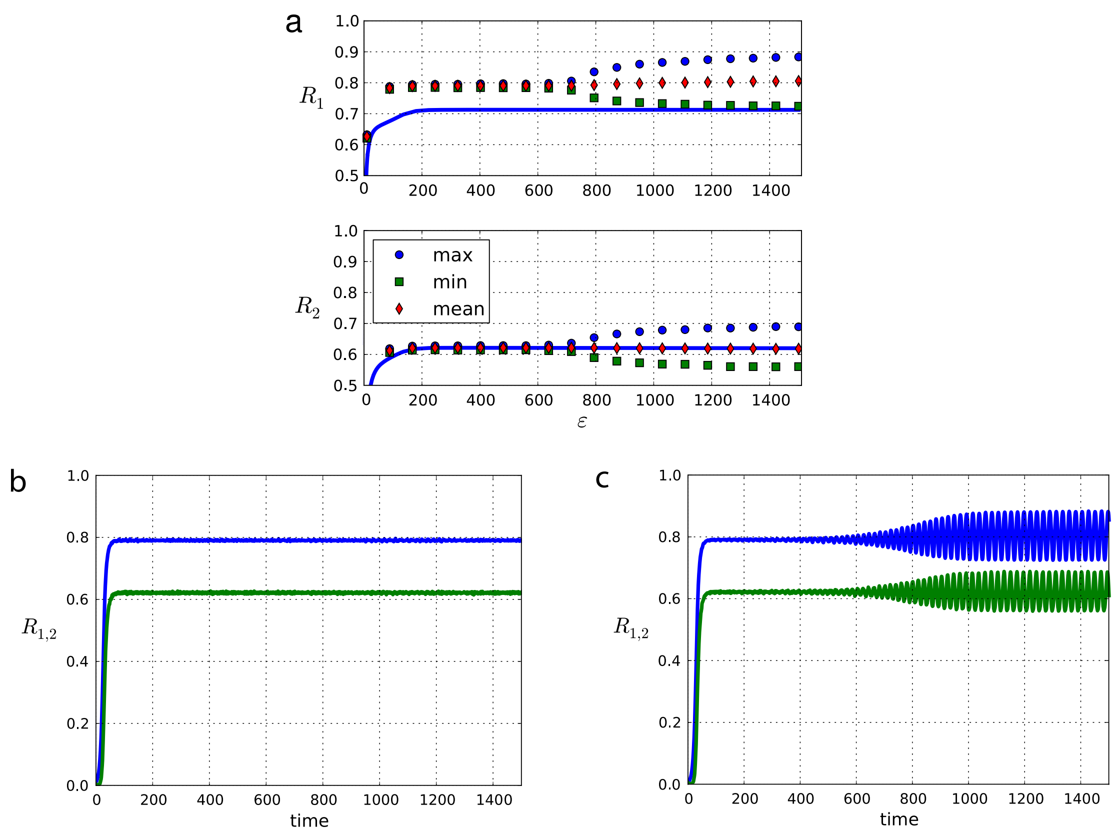

Fig. 10. (a) Lines are solutions of self-consistent equations (15)–(17) at $\beta_1 = \pi/2.5$, $\beta_2 = \pi$ and $\varepsilon/\gamma = 4$. Markers (showing maximum, minimum and mean values of $R_{1,2}$ calculated from time series after some transient period) depict results of direct numerical simulation of Eqs. (1) at the same parameters for $N = 2 \times 10^4$. The stationary state loses stability at a large coupling strength $\varepsilon \approx 650$, beyond which stable oscillations appear. (b, c) Time series of $R_{1,2}$ at different coupling strengths are presented: in the panel (b) $\varepsilon = 323$, in panel (c) $\varepsilon = 1420$.

of possible order parameters for given coupling constants. We have incorporated this multiplicity of multi-branch states into an analysis of self-consistent equations for the order parameters, and presented a general analytic solution.

2. Appearance of the synchronous states is not related to a standard bifurcation, as the asynchronous state does not change its neutral linear stability. We have found domains on the plane of basic coupling constants for the existence of such solutions, for different distributions of the locked phases between the branches (Fig. 2).
3. When a synchronous state is present, numerical experiments with finite ensembles show that the asynchronous state lives a finite time that scales like $T \sim N^{0.7}$, after which an abrupt transition to synchrony occurs. Similarly, we checked numerically stability of the states with single- and multi-branch entrainment through simulations of finite ensembles (Fig. 3).
4. At asymmetric distribution between the branches, the frequency of the order parameters deviates from the central frequency of the distribution, even if the latter and the coupling are symmetric.

Below we outline some open questions deserving further analysis. In the case of a general multi-harmonic coupling function Γ, one can expect existence of more than two stable branches for oscillators at a particular frequency, with more possibilities for different redistributions of the oscillators' phases. Another feature not addressed in this paper is related to the possibility of non-standard transitions to synchronize for particular distributions of the natural frequencies, similar to the analysis presented in Ref. [19] for the one-harmonic coupling. Detailed theoretical understanding of stability of the asynchronous states constructed via the self-consistency approach in this paper, is still missing. Finally, noise regularizes the multiplicity of the micro-states and turns neutral stability into an asymptotic one [41,20]; these effects will be discussed in details elsewhere [22].

Acknowledgments

M. K. thanks Alexander von Humboldt Foundation for support. AP and MK have been supported by the grant Nr 02..49.21.0003 (the agreement of August 27, 2013 between the Ministry of Education and Science of the Russian Federation and Lobachevsky State University of Nizhni Novgorod). We acknowledge useful discussions with V. Vlasov, M. Rosenblum, G. Bordyugov, R. Toenjes, and useful comments of S. Strogatz.

Appendix

Let us consider a system of N pendulums (with mass m and length l, described by angles θ_j) suspended on a beam of mass M, which can move vertically (axis y) and horizontally (axis x) without rotation. These motions are controlled by two springs k_x and k_y. This conservative system is described by the Lagrangian (cf. [42,33])

$$\begin{aligned} L = {} & \frac{M}{2}\left(\dot{x}^2 + \dot{y}^2\right) \\ & + \frac{m}{2}\sum_j \left(\dot{x}^2 + \dot{y}^2 + l\dot{x}\dot{\theta}_j \cos\theta_j - l\dot{y}\dot{\theta}_j \sin\theta_j + l^2\dot{\theta}_j^{\,2}\right) \\ & + mgl\sum_j \cos\theta_j + gy\,(Nm + M) - \frac{k_x x^2}{2} - \frac{k_y y^2}{2}. \end{aligned}$$

The equations are two equations for the degrees of freedom of the beam (where we shift y to the steady position $g(Nm+M)/ky$), and for each pendulum:

$$(M+Nm)\ddot{x}+k_x x=\sum_j -\frac{ml}{2}\ddot{\theta}_j\cos\theta_j+\sum_j\frac{ml}{2}\dot{\theta}_j^{\,2}\sin\theta_j$$

$$(M+Nm)\ddot{y}+k_y y=\sum_j \frac{ml}{2}\ddot{\theta}_j\sin\theta_j+\sum_j\frac{ml}{2}\dot{\theta}_j^{\,2}\cos\theta_j$$

$$ml^2\ddot{\theta}_j+mgl\sin\theta_j=\frac{ml}{2}\ddot{y}\sin\theta_j-\frac{ml}{2}\ddot{x}\cos\theta_j.$$

In order to model self-sustained oscillations of the pendulum clocks, we add dissipation terms ($\sim\gamma_{x,y}$) to beam equations, and van der Pol-type self-excitation terms $\sim\sigma$, together with cubic saturation, to the pendula dynamics. In the case of small deviations $\theta_{1,2}$ (i.e. for $\sigma/\rho\ll 1$) we have:

$$(M+Nm)\ddot{x}+\gamma_x\dot{x}+k_x x=\sum_j -\frac{ml}{2}\ddot{\theta}_j+\sum_j\frac{ml}{2}\dot{\theta}_j^{\,2}\theta_j \tag{29}$$

$$(M+Nm)\ddot{y}+\gamma_y\dot{y}+k_y y=\sum_j \frac{ml}{2}\ddot{\theta}_j\theta_j+\sum_j\frac{ml}{2}\dot{\theta}_j^{\,2} \tag{30}$$

$$\ddot{\theta}_j-(\sigma-\rho\theta_j^2)\dot{\theta}_j+\omega^2\theta_j=\frac{1}{2l}\ddot{y}\theta_j-\frac{1}{2l}\ddot{x} \tag{31}$$

where $\omega^2=g/l$.

For small $\sigma\ll\omega$ we can apply the averaging (van der Pol) method. We will seek for a solution of the form:

$$\theta_j=A_je^{i\omega t}+A_j^*e^{-i\omega t},\qquad \dot{\theta}_j=i\omega(A_je^{i\omega t}-A_j^*e^{-i\omega t})$$

where A_j are slowly varying in time amplitudes.

Using this representation, we can express the driving terms in the equations for the beam as follows:

$$\frac{ml}{2}\ddot{\theta}_j=-\frac{ml\omega^2}{2}\left(A_je^{i\omega t}+A_j^*e^{-\omega t}\right)$$

$$\begin{aligned}\frac{ml}{2}\dot{\theta}_j^{\,2}\theta_j&=-\frac{ml\omega^2}{2}\\&\times\left(A_j^3e^{3\omega t}-|A|_j^2A_je^{i\omega t}-A_j^*|A|_j^2e^{-i\omega t}+(A_j^*)^3e^{-3\omega t}\right)\end{aligned}$$

$$\frac{ml}{2}\ddot{\theta}_j\theta_j=-\frac{ml\omega^2}{2}\left(A_j^2e^{2i\omega t}+2|A|_j^2+(A_j^*)^2e^{-2\omega t}\right)$$

$$\frac{ml}{2}\dot{\theta}_j^2=-\frac{ml\omega^2}{2}\left(A_j^2e^{2i\omega t}-2|A_j|^2+(A_j^*)^2e^{-2i\omega t}\right)$$

Now the response of the beam to this driving can be expressed via solution of the linear equations, where the amplitudes A are considered as constants:

$$\begin{aligned}x(t)&=\sum_j\frac{ml\omega^2}{2}[H_x(\omega)A_j(1+|A|_j^2)e^{i\omega t}\\&\quad+H_x^*(\omega)A_j^*(1+|A_j|^2)e^{-i\omega t}\\&\quad-\left(H_x(3\omega)A_j^3e^{3\omega t}+H_x^*(3\omega)(A_j^*)^3e^{-3\omega t}\right)]\end{aligned}$$

$$y(t)=\sum_j -ml\omega^2\left[H_y(2\omega)A_j^2e^{2i\omega t}+H_y^*(2\omega)(A_j^*)^2e^{-2i\omega t}\right]$$

and for the second derivatives we get

$$\begin{aligned}\ddot{x}(t)&=\sum_j-\frac{ml\omega^4}{2}[H_x(\omega)A_j(1+|A|_j^2)e^{i\omega t}\\&\quad+H_x^*(\omega)A_j^*(1+|A_j|^2)e^{-i\omega t}\\&\quad-9\left(H_x(3\omega)A_j^3e^{3\omega t}+H_x^*(3\omega)(A_j^*)^3e^{-3\omega t}\right)]\end{aligned}$$

$$\ddot{y}(t)=\sum_j 4ml\omega^4\left[H_y(2\omega)A_j^2e^{2i\omega t}+H_y^*(2\omega)(A_j^*)^2e^{-2i\omega t}\right].$$

Here $H_{x,y}(\omega)$ are the response functions for the linear oscillators:

$$H_{x,y}(\omega)=\frac{1}{-\omega^2(M+Nm)+i\gamma_{x,y}\omega+k_{x,y}}.$$

Equations for the complex amplitudes $A_j(t)$ follow from rewriting Eq. (31) in terms of A_j and averaging it over the fast time (basic period $2\pi/\omega$):

$$\dot{A}_j=\frac{1}{2}A_j\left(\sigma-\rho|A_j|^2\right)+\frac{1}{4i\omega l}\langle\ddot{y}\theta_je^{-i\omega t}\rangle-\frac{1}{4i\omega l}\langle\ddot{x}e^{-i\omega t}\rangle.$$

After averaging only the terms with $\ddot{y}\theta_j\sim e^{i\omega t}$ and $\ddot{x}\sim e^{i\omega t}$ survive:

$$\dot{A}_j=\frac{1}{2}A_j\left(\sigma-\rho|A_j|^2\right)+DA_j^*\sum_k A_k^2+S\sum_k A_k$$

where

$$D=-im\omega^3H_y(2\omega),\qquad S=-\frac{im\omega^3}{8}H_x(\omega)$$

(here we neglected terms containing higher orders in A_j, due to smallness of the amplitudes). Terms $\sim D$ arise from the vertical motion of the beam $\ddot{y}$, while terms $\sim S$ are due to the horizontal motion $\ddot{x}$.

In the phase approximation we assume that the amplitudes $|A_j|$ are nearly constants $|A_j|=\sqrt{\sigma/\rho}$ and the interaction does not affect their dynamics. Therefore for phases ϕ_j ($A_j=|A_j|e^{i\phi_j}$) we have the following equations:

$$\dot{\phi}_j=\Omega+d\sum_k\sin(2(\phi_k-\phi_j)+\beta)+s\sum_k\sin(\phi_k-\phi_j+\alpha) \tag{32}$$

where $d=\sigma\rho^{-1}|D|$, $s=|S|$, $\beta=arg(D)$ and $\alpha=arg(S)$. The frequency is determined as $\Omega=\operatorname{Im}\left(\sigma\rho^{-1}D+S\right)$. The obtained system is the Kuramoto model with bi-harmonic coupling.

References

[1] K. Wiesenfeld, J.W. Swift, Averaged equations for Josephson junction series arrays, Phys. Rev. E 51 (2) (1995) 1020–1025.
[2] K. Wiesenfeld, P. Colet, S.H. Strogatz, Synchronization transition in a disordered Josephson series array, Phys. Rev. Lett. 76 (3) (1996) 404–407.
[3] K. Wiesenfeld, P. Colet, S. Strogatz, Frequency locking in Josephson arrays: Connection with the Kuramoto model, Phys. Rev. E 57 (2) (1998) 1563–1569.
[4] I. Kiss, Y. Zhai, J. Hudson, Emerging coherence in a population of chemical oscillators, Science 296 (2002) 1676–1678.
[5] J. Grollier, V. Cros, A. Fert, Synchronization of spin-transfer oscillators driven by stimulated microwave currents, Phys. Rev. B 73 (2006) 060409(R).
[6] B. Georges, J. Grollier, V. Cros, A. Fert, Impact of the electrical connection of spin transfer nano-oscillators on their synchronization: an analytical study, Appl. Phys. Lett. 92 (23) (2008) 232504.
[7] B. Eckhardt, E. Ott, S.H. Strogatz, D.M. Abrams, A. McRobie, Modeling walker synchronization on the Millennium Bridge, Phys. Rev. E 75 (2007) 021110.
[8] Z. Néda, E. Ravasz, T. Vicsek, Y. Brechet, A.L. Barabási, Physics of the rhythmic applause, Phys. Rev. E 61 (2000) 6987–6992.
[9] D. Golomb, D. Hansel, G. Mato, Mechanisms of synchrony of neural activity in large networks, in: F. Moss, S. Gielen (Eds.), Neuro-informatics and Neural Modeling, in: Handbook of Biological Physics, vol. 4, Elsevier, Amsterdam, 2001, pp. 887–968.
[10] M. Breakspear, S. Heitmann, A. Daffertshofer, Generative models of cortical oscillations: neurobiological implications of the Kuramoto model, Front. Hum. Neurosci. 4 (2010) 190.
[11] D. Gonze, S. Bernard, C. Waltermann, A. Kramer, H. Herzel, Spontaneous synchronization of coupled circadian oscillators, Biophys. J. 89 (1) (2005) 120–129.
[12] G. Bordyugov, P. Westermark, A. Korencic, H. Herzel, Mathematical modelling in chronobiology, in: A. Kramer, M. Merrow (Eds.), Circadian Clocks, Springer, 2013.
[13] Y. Kuramoto, Chemical Oscillations, Waves and Turbulence, Springer, Berlin, 1984.
[14] A. Pikovsky, M. Rosenblum, J. Kurths, Synchronization. A Universal Concept in Nonlinear Sciences, Cambridge University Press, Cambridge, 2001.
[15] Y. Kuramoto, Self-entrainment of a population of coupled nonlinear oscillators, in: H. Araki (Eds.) International Symposium on Mathematical Problems in Theoretical Physics, Springer Lecture Notes Phys., vol. 39, New York, 1975, p. 420.

[16] J.A. Acebrón, L.L. Bonilla, C.J.P. Vicente, F. Ritort, R. Spigler, The Kuramoto model: A simple paradigm for synchronization phenomena, Rev. Modern Phys. 77 (1) (2005) 137–175.
[17] E. Ott, T.M. Antonsen, Low dimensional behavior of large systems of globally coupled oscillators, Chaos 18 (3) (2008) 037113.
[18] E. Ott, T.M. Antonsen, Long time evolution of phase oscillator systems, Chaos 19 (2) (2009) 023117.
[19] O.E. Omel'chenko, M. Wolfrum, Nonuniversal transitions to synchrony in the Sakaguchi–Kuramoto model, Phys. Rev. Lett. 109 (2012) 164101.
[20] M. Komarov, A. Pikovsky, Multiplicity of singular synchronous states in the Kuramoto model of coupled oscillators, Phys. Rev. Lett. 111 (2013) 204101.
[21] K. Li, S. Ma, H. Li, J. Yang, Transition to synchronization in a kuramoto model with the first- and second-order interaction terms, Phys. Rev. E 89 (2014) 032917.
[22] V. Vlasov, M. Komarov, A. Pikovsky, unpublished (2014).
[23] H. Sakaguchi, Y. Kuramoto, A soluble active rotator model showing phase transition via mutual entrainment, Progr. Theoret. Phys. 76 (3) (1986) 576–581.
[24] J.D. Crawford, Scaling and singularities in the entrainment of globally coupled oscillators, Phys. Rev. Lett. 74 (21) (1995) 4341–4344.
[25] J.D. Crawford, K.T.R. Davies, Synchronization of globally coupled phase oscillators: singularities and scaling for general couplings, Physica D 125 (1–2) (1999) 1–46.
[26] H. Daido, Onset of cooperative entrainment in limit-cycle oscillators with uniform all-to-all interactions: bifurcation of the order function, Physica D 91 (1996) 24–66.
[27] H. Chiba, I. Nishikawa, Center manifold reduction for large populations of globally coupled phase oscillators, Chaos 21 (4) (2011) 043103.
[28] A.T. Winfree, The Geometry of Biological Time, Springer, Berlin, 1980.
[29] H. Daido, Multi-branch entrainment and multi-peaked order-functions in a phase model of limit-cycle oscillators with uniform all-to-all coupling, J. Phys. A: Math. Gen. 28 (1995) L151–L157.
[30] H. Daido, Multibranch entrainment and scaling in large populations of coupled oscillators, Phys. Rev. Lett. 77 (7) (1996) 1406–1409.
[31] D. Hansel, G. Mato, C. Meunier, Clustering and slow switching in globally coupled phase oscillators, Phys. Rev. E 48 (1993) 3470–3477.
[32] P.S. Skardal, E. Ott, J.G. Restrepo, Cluster synchrony in systems of coupled phase oscillators with higher-order coupling, Phys. Rev. E 84 (2011) 036208.
[33] K. Czolczyński, P. Perlikowski, A. Stefański, T. Kapitaniak, Synchronization of the self-excited pendula suspended on the vertically displacing beam, Commun. Nonlinear Sci. Numer. Simul. 18 (2) (2013) 386–400.
[34] E. Goldobin, D. Koelle, R. Kleiner, R.G. Mints, Josephson junction with a magnetic-field tunable ground state, Phys. Rev. Lett. 107 (2011) 227001.
[35] I.Z. Kiss, Y. Zhai, J.L. Hudson, Predicting mutual entrainment of oscillators with experiment-based phase models, Phys. Rev. Lett. 94 (2005) 248301.
[36] I.Z. Kiss, Y. Zhai, J.L. Hudson, Characteristics of cluster formation in a population of globally coupled electrochemical oscillators: An experiment-based phase model approach, Progr. Theoret. Phys. Suppl. 161 (2006) 99–106.
[37] S.H. Strogatz, R.E. Mirollo, Stability of incoherence in a population of coupled oscillators, J. Stat. Phys. 63 (3/4) (1991) 613–635.
[38] N.G.V. Kampen, On the theory of stationary waves in plasmas, Physica 21 (1955) 949–963.
[39] H. Daido, Generic scaling at the onset of macroscopic mutual entrainment in limit-cycle oscillators with uniform all-to-all coupling, Phys. Rev. Lett. 73 (5) (1994) 760–763.
[40] P. Ashwin, G. Orosz, J. Wordsworth, S. Townley, Dynamics on networks of cluster states for globally coupled phase oscillators, SIAM J. Appl. Dyn. Syst. 6 (4) (2007) 728–758. http://dx.doi.org/10.1137/070683969.
[41] T. Aonishi, M. Okada, Multibranch entrainment and slow evolution among branches in coupled oscillators, Phys. Rev. Lett. 88 (2001) 024102.
[42] M. Kapitaniak, K. Czolczyński, P. Perlikowski, A. Stefański, T. Kapitaniak, Synchronization of clocks, Phys. Rep. 517 (1–2) (2012) 1–69.